

# COSMOGLOBE DR1. III. First full-sky model of polarized synchrotron emission from all WMAP and Planck LFI data

D. Watts<sup>1\*</sup> and U. Fuskeland<sup>1</sup> et al.

Institute of Theoretical Astrophysics, University of Oslo, Blindern, Oslo, Norway

August 19, 2023

## ABSTRACT

We present the first statistically consistent model of full-sky polarized synchrotron emission derived from the combination of all *WMAP* and *Planck* LFI frequency maps. The basis of this analysis are the end-to-end reprocessed COSMOGLOBE Data Release 1 sky maps presented in a companion paper, which have significantly lower instrumental systematics than the legacy products from each experiment. We find that the resulting polarized synchrotron amplitude map has an average noise rms of  $2.4\mu\text{K}$  at 22 GHz and a smoothing scale of  $2^\circ$  FWHM, which is 30 % lower than the recently released BEYONDPLANCK model that included only LFI+*WMAP*  $Ka-V$  data, and it is 45 % lower than the raw *WMAP*  $K$ -band. The mean  $EE/BB$  power spectrum ratio is  $0.27 \pm 0.02$ , which agrees well with previous estimates from both *Planck* and QUIJOTE. Assuming a power law model for the synchrotron spectral energy density, we find a full-sky inverse noise-variance weighted mean of  $\beta_s = -3.06 \pm 0.08$  between *WMAP*  $K$ -band and LFI 30 GHz, in good agreement with previous estimates. At high Galactic latitudes, however, we find  $\beta_s = -3.31 \pm 0.08$ , which is slightly steeper than most previous foregrounds-oriented estimates, but in good agreement with the *Planck* 2018 LFI CMB likelihood result of  $\beta_s = -3.27 \pm 0.04$ . For comparison, the corresponding full-sky and high-latitude estimates derived from the official *WMAP* and LFI products are  $\beta_s = -3.44 \pm 0.08$  and  $\beta_s = -3.71 \pm 0.08$ , respectively. These values are obviously compromised by large-scale instrumental systematics in both *WMAP* and LFI. In summary, the novel COSMOGLOBE DR1 synchrotron model is both more sensitive and systematically cleaner than similar previous models, and it has a more complete error description that is defined by a set of Monte Carlo posterior samples. We believe that these products are preferable for all synchrotron-related scientific applications, including simulation, forecasting and component separation.

**Key words.** ISM: general – Cosmology: observations, polarization, cosmic microwave background, diffuse radiation – Galaxy: general

## Contents

<b>1</b>	<b>Introduction</b>	many others, the future LiteBIRD satellite and ground-based Simons Observatory (SO) and CMB-S4 experiments will create
<b>2</b>	<b>Data products</b>	the most sensitive maps of the polarized sky yet, providing the most stringent constraints on primordial gravitational waves.
2.1	<i>WMAP</i> and <i>Planck</i> legacy products . . . . .	<b>2</b> In the past decade, uncertainty on cosmological constraints
2.2	<i>COSMOGLOBE</i> products . . . . .	<b>2</b> has been limited not only by instrumental sensitivity, but by incomplete knowledge of the sky itself. These analysis difficulties have been mitigated by analyzing maps from different experiments, e.g., <a href="#">BICEP2/Keck Array</a> and <a href="#">Planck Collaborations (2015)</a> , or designing of experiments with broad frequency coverage, such as <i>WMAP</i> ( <a href="#">Bennett et al. 2013</a> ) and <i>Planck</i> ( <a href="#">Planck Collaboration I 2020</a> ). A major impediment to joint analyses is
<b>3</b>	<b>Polarized synchrotron amplitude</b>	<b>4</b> the difficulty of combining data with different survey strategies
3.1	Power spectra . . . . .	<b>4</b> and incompletely characterized systematics. In order to maximize scientific throughput, one must either design an experiment
3.2	Comparison with independent datasets . . . . .	<b>5</b> that can characterize every relevant observable on its own, or
<b>4</b>	<b>Polarized synchrotron spectral indices</b>	<b>5</b> jointly analyze different datasets in the same joint framework.
4.1	TT-plot method . . . . .	
4.2	Maximum likelihood estimation . . . . .	
<b>5</b>	<b>Discussion and conclusion</b>	

## 1. Introduction

Understanding the polarization of the cosmic microwave background (CMB) is a primary focus of observational cosmology in the coming decades. Following the success of the satellite-based COBE, *WMAP*, and *Planck* experiments, as well as sub-orbital experiments including, e.g., BICEP, ACT, SPT, Polarbear, and

\* Corresponding author: D. Watts; [duncanwa@astro.uio.no](mailto:duncanwa@astro.uio.no)

The BEYONDPLANCK project achieved this joint analysis by combining external data, i.e., the Haslam 408 MHz map ([Haslam et al. 1982](#)), *WMAP*  $Ka-V$  bands, *Planck* 353 GHz in polarization, and *Planck* 857 GHz in intensity, while analyzing the *Planck* 30, 44, and 70 GHz TOD ([BeyondPlanck Collaboration 2023](#)). The *Planck* LFI experiment showed that raw detector sensitivity was not enough to obtain high-fidelity sky maps; [Planck Collaboration II \(2020\)](#) found that the detector gain solution depended on the assumed polarization and intensity of the sky. To break this circular dependency, the BEYONDPLANCK

framework solved for the intrinsic sky signal and instrumental parameters iteratively, providing an accurate model of the entire system with full error propagation. By leveraging external data, BEYONDPLANCK was able to create *Planck* LFI maps of cosmological quality, while generating a robust model of the foreground sky.

In COSMOGLOBE DR1 (Watts et al. 2023a), this end-to-end framework was extended, performing a joint analysis of the same data as BEYONDPLANCK while adding the full *WMAP* time-ordered data. This analysis not only improved the quality of the *WMAP* maps themselves, but provided the most robust full-sky model of low frequency polarized emission available to date.

In order to make use of the synchrotron model, we require robust estimates of the spectral behavior. Fundamental behaviors, such as the spectral index as a function of frequency, spatial decorrelation, and even the functional form of the SED, are yet to be fully characterized observationally. Modern attempts have been stymied by the lack of high signal-to-noise data; de Bel-sunce et al. (2022), for example, find spectral indices ranging from  $-5$  to  $-1$ , well outside of the theoretical limits of (?), given in, e.g., (?). This discrepancy is largely due to inadequate data coverage, requiring higher signal-to-noise datasets that have not yet been generated. Therefore, any conclusions about the distribution of the polarized synchrotron spectral index must be verified through multiple independent analysis methods and data choices.

While the combination of as many datasets as possible would help to constrain polarized synchrotron's large-scale properties, long-standing discrepancies complicates this. As shown in, e.g., Planck Collaboration X (2016) and Weiland et al. (2018), there are discrepancies in the polarization measurements of *WMAP* and *Planck*, partially due to unconverged gain solutions (Planck Collaboration II 2020) and poorly measured mapmaking modes (Bennett et al. 2013). BeyondPlanck Collaboration (2023) resolved the unconverged gain solution creating low-systematics LFI maps for the first time, while Watts et al. (2023b) demonstrated that the poorly measured modes in *WMAP* could be removed through joint processing, while identifying a similar systematic effect that could mimic the previously-reported effect. While Watts et al. (2023a) has demonstrated that the polarized maps from these two experiments are now consistent at the white noise level, the new maps must be validated first. As noted in, e.g., Weiland et al. (2022), simply using a different LFI pipeline can result in non-physical sky components.

In this work, we will use the *WMAP* and LFI maps generated in the COSMOGLOBE DR1 analysis. We perform three separate analyses; a map and power spectrum-based analysis of the synchrotron amplitude, linear correlation within regions (T-T plots), and per-pixel Gibbs sampling.

For the power spectra, compare with, e.g., Figure 33 of Planck Collaboration IV (2018). We use the same bins as in Table C.1 of Planck Collaboration XI (2020)

## 2. Data products

In this paper, we investigate the spatial variation of the polarized synchrotron spectral index, with an emphasis on the comparison between legacy maps against the COSMOGLOBE results. The data products used are the *WMAP* and *Planck* LFI maps, with most of the statistical weight coming from 23–33 GHz. These frequencies are low enough that we can treat them as synchrotron tracers and hence ignore thermal dust and CMB, but not so low as we need to take into account effects like Faraday rotation (Fuskeland et al. 2021). The legacy data products and the data products

from the COSMOGLOBE *WMAP* reanalysis (Watts et al. 2023a), are described in the two following sections.

### 2.1. WMAP and Planck legacy products

The *Wilkinson Microwave Anisotropy Probe* (Bennett et al. 2013, *WMAP*) was a NASA-funded satellite mission that observed from August 2001 to August 2010, designed to characterize the microwave sky well enough to measure the primary CMB anisotropies across the full sky down to a resolution of  $13'$ . Using a differential scanning strategy inspired by *COBE*/DMR, *WMAP* produced maps of the sky at 23 (*K*), 33 (*Ka*), 41 (*Q*), 61 (*V*), and 94 GHz (*W*) in both polarization and intensity (Bennett et al. 2013), with angular resolutions of  $53'$  at 23 GHz to  $13'$  at 94 GHz. The maps are available on the LAMBDA website.<sup>1</sup>

The *Planck* Low Frequency Instrument (LFI) produced 30, 44, and 70 GHz maps in both intensity and polarization, while the High Frequency Instrument (HFI) produced 100, 143, 217, 353 GHz maps in polarization and intensity, and 545 and 857 GHz maps in intensity alone. The LFI data in particular are similar to the *WMAP* data, with higher angular resolutions of  $30'$ ,  $20'$ , and  $13'$  for 30, 44, and 70 GHz, and with higher sensitivity. Although the detector design was similar, LFI observed with a single horn, and observed in rings closely aligned with the ecliptic longitude. The legacy datasets, PR3 (Planck Collaboration I 2020) and PR4 (Planck Collaboration Int. LVII 2020), are both publicly available on the *Planck* Legacy Archive (PLA).<sup>2</sup>

### 2.2. COSMOGLOBE products

The goal of COSMOGLOBE is to perform joint end-to-end analyses on several data sets jointly, preferably beginning from raw time-ordered data (TOD). Doing this can help to break the degeneracies of the different data sets, and in general reduced the amplitude of systematic effects. The analysis in BeyondPlanck Collaboration (2023) and Watts et al. (2023a) was performed on raw TOD to cosmological parameters using the Bayesian Gibbs sampler, Commander3. The data products produced in these analysis account for the complex interactions between the instrument, the microwave sky, and its consistent components self-consistently. The full products from this analysis and individual maps are available on the COSMOGLOBE website.<sup>3</sup>

The analysis in this paper makes use of COSMOGLOBE end products produced by the reanalysis of the *WMAP* and *Planck* LFI TODs (Watts et al. 2023a). This analysis produced improved *WMAP* and *Planck* LFI maps, which we will use in an analysis to compare to the legacy data. In particular, we are interested in exactly the same set of maps as in the previous section in order to be able to do a comparision study. The pixelization and angular scale are the same as for the legacy products ( $N_{\text{side}} = 64$ ,  $1^\circ$  FWHM). The COSMOGLOBE end products consists of a series of 500 samples from the Gibbs chain, instead of just one mean sample as has been the normal case for previous data releases.

## 3. Polarized synchrotron amplitude

COSMOGLOBE DR1 produced a sky model and instrumental parameters for each Gibbs sample, allowing for complete charac-

<sup>1</sup> [https://lambda.gsfc.nasa.gov/product/wmap/dr5/m\\_products.html](https://lambda.gsfc.nasa.gov/product/wmap/dr5/m_products.html)

<sup>2</sup> <https://pla.esac.esa.int/>

<sup>3</sup> <https://www.cosmoglobe.uio.no/products/cosmoglobe-dr1.html>



**Fig. 1.** Polarized intensity of (top): WMAP  $K$ -band, (middle): *Planck* 30 GHz, and (bottom): synchrotron amplitude from COSMOGLOBE Gibbs chain, all evaluated at 30 GHz with a resolution of  $72'$ . The right column shows the rms noise for the frequency maps and the posterior standard deviation of the synchrotron amplitude.

terization of the dependence of low-level instrumental parameters on the sky model. The sky model includes all relevant components in *WMAP* and LFI's frequency range, specifically the CMB, synchrotron, thermal dust, free-free emission, anomalous microwave emission, and radio point sources, the first three of which are known to be polarized.

When using external data for polarized foreground cleaning, the choices for high signal-to-noise full sky constraints are either *WMAP*  $K$ -band, *Planck* LFI 30 GHz, or models derived from combinations of these data, as in, e.g., COSMOGLOBE. From the perspective of pure statistical uncertainty, a combination of multiple independent datasets would yield component maps that are more sensitive than each individual component. However, unmodeled systematic uncertainties in the underlying datasets, left untreated, can induce map effects that can leak into astrophysics and cosmological constraints. As shown in Watts et al. (2023a), a single sky model that all datasets are calibrated against improves the low-level instrumental processing, and allowing for degeneracies, such as poorly-measured modes in *WMAP* and differential gain uncertainty in LFI, to be broken. Within the COSMOGLOBE DR1 framework, the polarization maps from *WMAP* and *Planck* LFI are consistent with each other at the  $10\,\mu\text{K}$  level, consistent with the instrumental white noise of the datasets.

The COSMOGLOBE DR1 frequency maps are free from previously reported systematics, and are consistent between different frequencies and instruments. Therefore, a coherent model of polarized synchrotron emission can be made by combining these two different datasets. The polarized spectral amplitude determined from COSMOGLOBE fully utilizes the *Planck* and *WMAP* joint reprocessed data, as shown in Fig. 1. We plot the total polarized amplitude  $P = \sqrt{Q^2 + U^2}$  for ease of comparison, although it creates a visible noise bias in the low signal-to-noise regions. Much of the constraining power in the polarized synchrotron amplitude comes from

While the COSMOGLOBE pipeline produces samples of polarized synchrotron emission, the spatial variation of the spectral index is poorly determined within the Gibbs chain. To mitigate the poor MCMC convergence of the spectral indices, the COSMOGLOBE DR1 sampled the spectral index from a prior distribution,  $\beta_s \sim N(-3.15, 0.05^2)$ . Improvements within the Commander3 framework will require more high signal-to-noise data and algorithmic improvements within the codebase.

The *WMAP*  $K$ -band data and LFI 30 GHz data, as the highest signal-to-noise full-sky polarized maps of Galactic synchrotron emission, are the main contributors to our knowledge of the polarized amplitude. The slightly higher angular resolution 30 GHz map has lower sensitivity than the  $K$ -band data, but by combin-



**Fig. 2.** COSMOGLOBE posterior standard deviation divided by BEYONDPLANCK posterior standard deviation. The ratio is less than one for all pixels.

ing the multi-resolution maps we are able to produce a clean map of the synchrotron emission evaluated at 30 GHz with a FWHM of  $1^\circ$ .

The synchrotron amplitude maps from end-to-end processing, BEYONDPLANCK and COSMOGLOBE, contain slightly different datasets, but sample the instrumental properties and sky properties jointly. Of these maps, BEYONDPLANCK has lower resolution and higher noise, in large part because COSMOGLOBE is able to use the reprocessed WMAP K-band map. The COSMOGLOBE synchrotron map has a mean posterior rms of  $2.4 \mu\text{K}$ , a marked improvement over the BEYONDPLANCK map, as shown in Fig. 2. The rms map itself contains high signal-to-noise regions corresponding to the WMAP circles about the ecliptic poles as well as the Planck rings and multiple ecliptic polar crossings. The main clear astrophysical variation comes in the forms of a thin region about the Galactic plane and several low-latitude point sources. Much of the improvement can be seen more clearly when taking the ratio of the posterior rms's, as in the bottom panel of Fig. 2. As expected, the regions with the lowest ratios correspond to the deep WMAP observations and the Galactic plane, which benefit from the high signal-to-noise of the K-band data. Regions with nearly identical rms include regions with the highest Planck depth, i.e., the ecliptic poles, and regions less deeply observed by WMAP, corresponding to planet crossings and artifacts from the processing mask. Notably, stripes corresponding the Planck scan strategy also show improvement respect to BEYONDPLANCK. This is due to the interaction between the sky model and LFI's instrumental parameters – with the high signal-to-noise K-band data, the sky model becomes more stable, and LFI's relative gain solution becomes better determined.

To quantify the noise improvement in the synchrotron maps over pure templates based on either K-band or 30 GHz maps, we compare the posterior standard deviation of the COSMOGLOBE synchrotron map with the frequency maps' rms values. The posterior standard deviation maps are  $\lesssim 1 \mu\text{K}$  for K-band, while temperature-to-polarization uncertainty in 30 GHz contributes at the  $2 \mu\text{K}$  level (see, e.g., Watts et al. 2023a and Basyrov et al. 2023 for further details). An informative prior of  $D_\ell = 200 e^{-\ell(\ell+1)\sigma^2(30')} \mu\text{K}^2$  is applied during polarized synchrotron amplitude fitting, essentially downweighting low signal-to-noise fluctuations at angular scales  $\lesssim 30'$ , or  $\ell \gtrsim 360$  (Svalheim et al. 2023). Therefore, the rms noise contributions are relevant at roughly  $N_{\text{side}} = 128$ . We additionally simulate white noise smoothed to  $72'$  and scaled to 30 GHz assuming  $\beta_s = -3.1$ , consistent with the post-processed synchrotron map, which we display in the right column of Fig. 1.

**Table 1.** Synchrotron power spectrum estimates

	PR3	COSMOGLOBE
$A_{\text{EE}}^{\text{EE}}$ . . . . .	$2.22 \pm 0.09$	$2.23 \pm 0.06$
$A_{\text{BB}}^{\text{BB}}$ . . . . .	$0.91 \pm 0.07$	$0.80 \pm 0.04$
$A_{\text{s}}^{\text{BB}} / A_s^{\text{EE}}$ . . . . .	$0.41 \pm 0.03$	$0.36 \pm 0.02$
$a_s^{\text{EE}}$ . . . . .	$-0.89 \pm 0.04$	$-0.93 \pm 0.04$
$a_s^{\text{BB}}$ . . . . .	$-0.86 \pm 0.07$	$-0.89 \pm 0.06$

At these resolutions, the mean rms for K-band and 30 GHz are  $4.8 \mu\text{K}$  and  $4.7 \mu\text{K}$  respectively, compared to the mean value of  $3.4 \mu\text{K}$  for the COSMOGLOBE DR1 synchrotron map, consistent with adding the scaled maps in quadrature. While this may seem obvious on its face, the combination of WMAP K-band and Planck 30 GHz is not straightforward due to instrumental effects that remain in the maps, notably poorly measured modes in WMAP (Bennett et al. 2013; Weiland et al. 2018) and gain uncertainty in Planck (Planck Collaboration II 2020). These effects remain in the official WMAP9 (Bennett et al. 2013) and Planck PR3/PR4 (Planck Collaboration II 2020; Planck Collaboration Int. LVII 2020) maps, making combination of these datasets unsuitable for Galactic science and cosmological analyses. However, the end-to-end BEYONDPLANCK (BeyondPlanck Collaboration 2023) products effectively removed the gain uncertainty modes from the Planck LFI maps, and the COSMOGLOBE DR1 results (Watts et al. 2023a) are free from the poorly measured modes. As shown in Fig. ??, the Planck 30 GHz and the WMAP K-band are consistent with each other at the  $10 \mu\text{K}$  level, indicating that the maps are consistent with each other down to the white noise level.

This polarized synchrotron map, derived from consistent datasets, has a white noise level 29 % lower than both the K-band map and the 30 GHz map, with minimal systematic uncertainties in the posterior standard deviation. Therefore, the synchrotron map derived from the COSMOGLOBE DR1 Gibbs chain should be used for the characterization and removal of polarized synchrotron emission between 23–90 GHz.

### 3.1. Power spectra

We needed to run a special Commander3 chain, splitting the TODs into half mission, with all odd-numbered scans being processed in chain “HM1”, and all even-numbered scans in “HM2”, and produced 200 samples each. We provide these data at [cosmoglobe.uio.no](http://cosmoglobe.uio.no).

We perform cross-spectra to avoid an additive noise bias.

We use NaMaster using the original chain. To quantify the uncertainty, we take the cross spectrum for each pair of Gibbs samples from the adjacent chain, and report the 68 % confidence intervals on this posterior. We find good agreement with the EE/BB ratio reported in Planck 2018 using their half-mission results. For the Planck data, we use standard deviation of the single- $\ell$  spectrum values within each bin, while we add the systematic quadrature from the COSMOGLOBE chain in quadrature. Compare with, e.g., Planck Collaboration X (2016)'s Figure 44.

### 3.2. Comparison with independent datasets

First, the residual maps at K, 30 GHz. Then compare the evaluated sky model with WMAP9's K-band map, PR3, and PR4.



**Fig. 3.** Half-mission splits of synchrotron for *Planck* PR3 (black) and COSMOGLOBE DR1 (black). Filled circles correspond to *E*-modes, while empty circles correspond to *B*-modes.



**Fig. 4.** The sky is split into the same 24 regions as in Fuskeland et al. (2014). The most prominent point sources are masked out and shown as grey circular areas.

#### 4. Polarized synchrotron spectral indices

As pointed out in Wehus et al. (2013), elliptical beams can induce a polarization angle-dependent spectral index for point sources, which can often be identified by performing analysis as a function of polarization angle. As both *WMAP* and *Planck* have asymmetric beam responses, this effect exists in the data, so spectral index estimation will be contaminated by this. Performing the TT analysis as a function of polarization angle, as discussed in Sec. 4.1, shows the magnitude of this effect in the COSMOGLOBE, *WMAP*9, and PR4 data.

##### 4.1. TT-plot method

Following Fuskeland et al. (2014) and Fuskeland et al. (2021), we apply linear regression via the T-T (“temperature-temperature”) method, in which spectral indices can be estimated over extended regions with approximately constant spectral indices. In this approach, our data model for two frequencies is

$$\mathbf{m}_\nu = \mathbf{m}_{\nu_0} \left( \frac{\nu}{\nu_0} \right)^\beta + o_\nu + \mathbf{n}_\nu, \quad (1)$$

where  $\mathbf{m}_\nu$  is a spatially varying amplitude map,  $\nu_0$  is the reference frequency,  $\beta$  the power law between the two frequencies,

$o_\nu$  the spatially constant offset per band, and  $\mathbf{n}_\nu$  the noise. In the case of noiseless data with no offset, the spectral index may be estimated using a simple ratio,

$$\frac{\mathbf{m}_{\nu_1,p}}{\mathbf{m}_{\nu_2,p}} = \left( \frac{\nu_1}{\nu_2} \right)^{\beta_{s,p}} \Rightarrow \beta_{s,p} = \frac{\ln(\mathbf{m}_{\nu_1,p}/\mathbf{m}_{\nu_2,p})}{\ln(\nu_1/\nu_2)}. \quad (2)$$

The standard T-T plot method computes performs a linear regression  $\mathbf{m}_{\nu_1} = a\mathbf{m}_{\nu_2} + b$ , and associates  $\beta_s$  with  $\ln a / \ln(\nu_1/\nu_2)$ . More care must be taken when the noise amplitudes in both maps are comparable, so we adopt the effective variance method of Orear (1982) as implemented by Fuskeland et al. (2014).

For the T-T plot analysis, we focus exclusively on bands between 23 and 33 GHz. As in Fuskeland et al. (2014), we use the *WMAP* *K* and *Ka* band Stokes *Q* and *U* parameter maps at 23 GHz and 33 GHz. The respective effective frequencies used are 22.45 GHz and 32.64 GHz. The maps originally at a HEALPix pixelization of  $N_{\text{side}} = 512$  are downgraded to  $N_{\text{side}} = 64$  and smoothed to a common resolution of  $1^\circ$  FWHM. The *Planck* data products used are the 30 GHz Stokes *Q* and *U* maps, with an effective frequency of 28.4 GHz. The COSMOGLOBE (PR4) products are natively at  $N_{\text{side}} = 512$  (1024), but as for the *WMAP* products, the maps are downgraded to  $N_{\text{side}} = 64$  and smoothed to  $1^\circ$  FWHM.

The uncertainty is calculated as the minimum of the uncertainties in each rotation angle, and region. As in the Fuskeland 2021 paper, an systematic uncertainty that takes into account the variation of  $\beta$  over rotation angle;  $[\max(\beta_\alpha) - \min(\beta_\alpha)]/2$  is added in quadrature to the statistical uncertainty. For the COSMOGLOBE analyses the standard deviation of the spectral indices for all samples is also added in quadrature to represent an additional systematic uncertainty.

Much better propagation of uncertainties with a whole suite of maps.

We will also use Table 6, Figure (33) of Planck 2018 results IV Diffuse component separation

#### 4.2. Maximum likelihood estimation

#### 5. Discussion and conclusion

#### References

- Basyrov, A., Suur-Uski, A.-S., Colombo, L. P. L., et al. 2023, A&A, 675, A10
- Bennett, C. L., Larson, D., Weiland, J. L., et al. 2013, ApJS, 208, 20
- BeyondPlanck Collaboration. 2023, A&A, 675, A1
- BICEP2/Keck Array and Planck Collaborations. 2015, Phys. Rev. Lett., 114, 101301
- de Belsunce, R., Gratton, S., & Efstathiou, G. 2022, MNRAS, 517, 2855
- Fuskeland, U., Andersen, K. J., Aurién, R., et al. 2021, A&A, 646, A69
- Fuskeland, U., Wehus, I. K., Eriksen, H. K., & Næss, S. K. 2014, ApJ, 790, 104
- Haslam, C. G. T., Salter, C. J., Stoffel, H., & Wilson, W. E. 1982, A&AS, 47, 1
- Orear, J. 1982, American Journal of Physics, 50, 912
- Planck Collaboration X. 2016, A&A, 594, A10
- Planck Collaboration I. 2020, A&A, 641, A1
- Planck Collaboration II. 2020, A&A, 641, A2
- Planck Collaboration IV. 2018, A&A, 641, A4
- Planck Collaboration XI. 2020, A&A, 641, A11
- Planck Collaboration Int. LVII. 2020, A&A, 643, A42
- Svalheim, T. L., Andersen, K. J., Aurién, R., et al. 2023, A&A, 675, A14
- Watts, D. J., Basyrov, A., Eskilt, J. R., et al. 2023a, arXiv e-prints, arXiv:2303.08095
- Watts, D. J., Galloway, M., Ihle, H. T., et al. 2023b, A&A, 675, A16
- Wehus, I. K., Fuskeland, U., & Eriksen, H. K. 2013, ApJ, 763, 138
- Weiland, J. L., Addison, G. E., Bennett, C. L., Halpern, M., & Hinshaw, G. 2022, ApJ, 936, 24
- Weiland, J. L., Osumi, K., Addison, G. E., et al. 2018, ApJ, 863, 161



**Fig. 5.** The spatial variation of the synchrotron spectral index, computed using T-T plot between the *WMAP9* 23 GHz and *Planck* 2018 30 GHz (top), *WMAP9* 23 GHz and *Planck* DR4 30 GHz (middle) and *COSMOGLOBE* 23 GHz and *COSMOGLOBE* 30 GHz (bottom). The spectral index is inverse variance weighted over rotation angle, and in the *COSMOGLOBE* case also samples. Fix style of maps. Bottom figure will be updated using more samples.



**Fig. 6.** The synchrotron spectral index as a function of region number, computed using T-T plot between the 9-yr *WMAP* 23 GHz and *Planck* 2018 30 GHz (red), 9-yr *WMAP* 23 GHz and *Planck* DR4 30 GHz (blue) and *COSMOGLOBE* 23 GHz and *COSMOGLOBE* 30 GHz (black). The spectral index is inverse variance weighted over rotation angles, and samples. The horizontal line in the high latitude regions corresponds to the estimated spectral index values from the *Planck* 2018 likelihood analysis. cite?? Figure will be updated using more samples.



**Fig. 7.** The synchrotron spectral index computed using T-T plot with the *COSMOGLOBE* 23 GHz and 30 GHz data versus *COSMOGLOBE* 23 GHz and 33 GHz data for the 24 regions. Figure will be updated using more samples.



**Fig. 8.** T-T plots for Stokes Q and U maps of the COSMOGLOBE 23 GHz versus the COSMOGLOBE 30 GHz (black) and the 9 yr WMAP 23 GHz versus Planck 2018 30 GHz (red) for all regions. The horizontal (solid and dotted) lines indicates the corresponding inverse variance weighted values of the spectral index, averaged over rotation angle. [Figure will be updated using more samples.](#)



**Fig. 9.** The synchrotron spectral index as a function of rotation angle, computed using T-T plot between the CosMOGLOBE 23 GHz and the CosMOGLOBE 30 GHz (black) compared to the spectral index using the 9 yr WMAP 23 GHz and *Planck* 2018 30 GHz (red) for all regions. The horizontal (solid and dotted) lines indicates the corresponding inverse variance weighted values of the spectral index. **Figure will be updated using more samples.**



**Fig. 10.** The spatial variation of the synchrotron spectral index, computed using T-T plot between the COSMOGLOBE WMAP  $K$ -band and  $Ka$ -band. The spectral index is inverse variance weighted over rotation angle and samples. **Fix style of maps. Figure will be updated using more samples.**



**Fig. 11.** The uncertainty of the synchrotron spectral index, computed using T-T plot between the COSMOGLOBE WMAP  $K$ -band and  $Ka$  band. **REMOVE? Figure will be updated using more samples.**

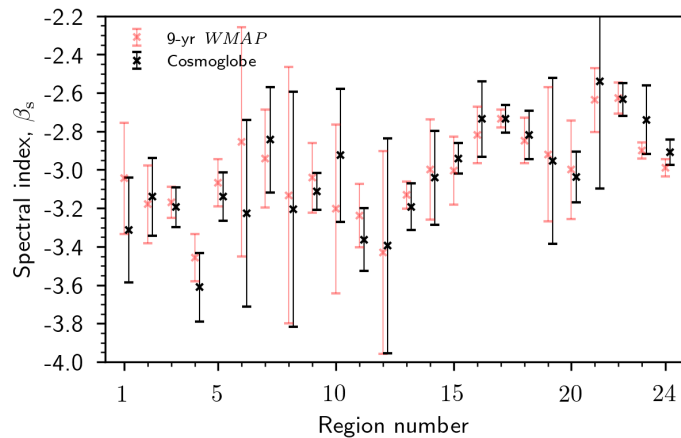


**Fig. 12.** The synchrotron spectral index, computed using T-T plot between the COSMOGLOBE WMAP  $K$ -band and  $Ka$ -band (red) compared to the spectral index using the original 9 yr WMAP data (black) as a function of region number. The spectral index is inverse variance weighted over rotation angles, and samples. **Figure will be updated, adding larger final uncertainty and using more samples.**



**Fig. 13.** The synchrotron spectral index as a function of rotation angle, computed using T-T plot between the Cosmoglobe WMAP  $K$ -band and  $Ka$ -band (red) compared to the spectral index using the original 9 yr WMAP data (black) for all regions. The horizontal lines indicates the corresponding inverse variance weighted values of the spectral index. **Figure will be updated using more samples.**